Supporting Information

Mechanism of Oxygen Evolution Catalyzed by Cobalt Oxyhydroxide: Cobalt Superoxide Species as a Key Intermediate and Dioxygen Release as a Rate-Determining Step

Aliki Moysiadou,[†,‡] Seunghwa Lee,[†,‡] Chia-Shuo Hsu,[§] Hao Ming Chen,[§] Xile Hu[†,]*

[†]Laboratory of Inorganic Synthesis and Catalysis, Institute of Chemical Sciences and Engineering, École Polytechnique Fédérale de Lausanne (EPFL), ISIC-LSCI, 1015 Lausanne, Switzerland

[§]Department of Chemistry, National Taiwan University, Taipei 10617, Taiwan

[‡] These authors contributed equally to this work

* E-mail: xile.hu@epfl.ch

1. Scanning Electron Microscopy

Thin films of CoOOH were electrodeposited by applying an anoidc durrent of 10 μA for 3 s. The metal loading was equal to 77.00±6.30 ppb according to ICP-OES analysis, which corresponded to 6.0±0.5 μg cm^{-2} assuming that the catalysts were deposited as oxyhydroxides. SEM images of smooth and nanostructured Au substrates revealed a much higher surface area for the latter. The ECSA of Au increased by ca. 50% after the roughening procedure as explained in section S2.1 (see below). The expected thickness of the films was ca. 2.0–2.5 nm.
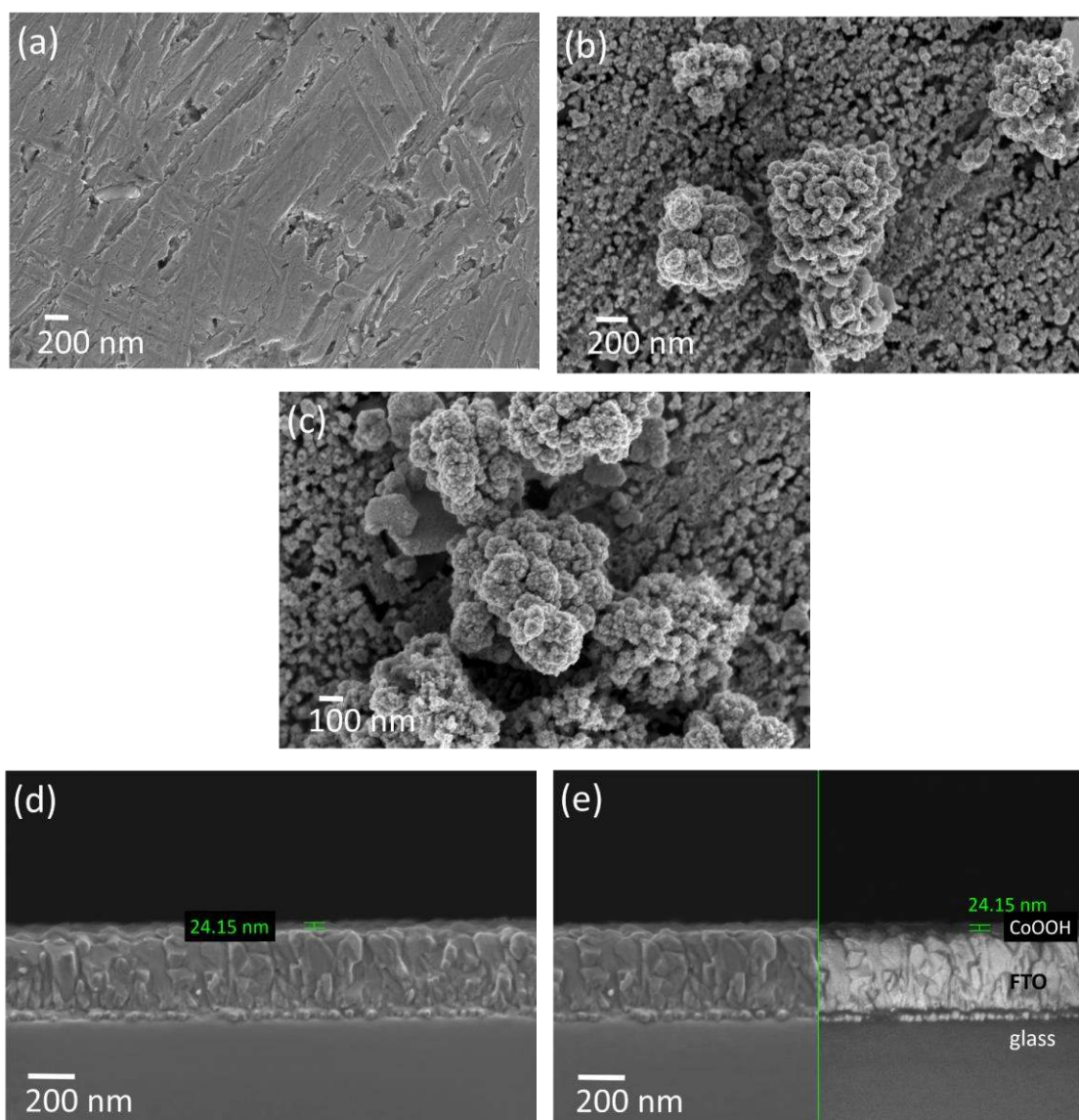

Figure S1. Secondary electron images of (a) smooth Au, (b, c) nanostructured Au, (d) cross section of CoOOH film deposited on a flat FTO/glass substrate (galvanostatic deposition at 10 μA for 3 min), (e) secondary and backscattered electron images of the CoOOH/FTO/glass cross section. The thickness on a flat surface (geometrical surface area: 0.1926 cm^2) is between 20-24 nm for 3 min deposition. The real surface area of our nanostructured Au (1.86 cm^2) is almost 9 times bigger than the geometrical surface area leading to an estimated thickness of 2.0–2.5 nm.

2. Electrochemical Surface Area measurements

2.1. Smooth and roughened Au substrates

The real surface area of Au was determined by cyclic voltammetry in 0.1 M phosphate buffer solutions (pH 7.4). The potential was cycled between the values of 0.5 and 1.9 V vs. RHE as shown in Figure S2a. The anodic peak corresponds to the oxidation of Au and the formation of an oxide layer, while the cathodic peak represents the reduction or stripping of the AuO layer. The stripping charge of the oxide was calculated by integrating the reduction peak appearing in the cathodic scan. The ECSA is equal to the stripping charge of the oxide, Q_{AuO} (μC), divided by 482 μC cm^{-2}, the theoretical mean surface concentration of gold atoms on a flat surface.[1] The electrochemical activity of nanostructured Au was investigated in 0.1 M Fe-free KOH as shown in Figure S2b. In the anodic scan, the gradual oxidation of gold to gold oxide starts at ca. 1.30 V, while the reduction/stripping of the oxide takes place at ca. 1.10–1.15 V.
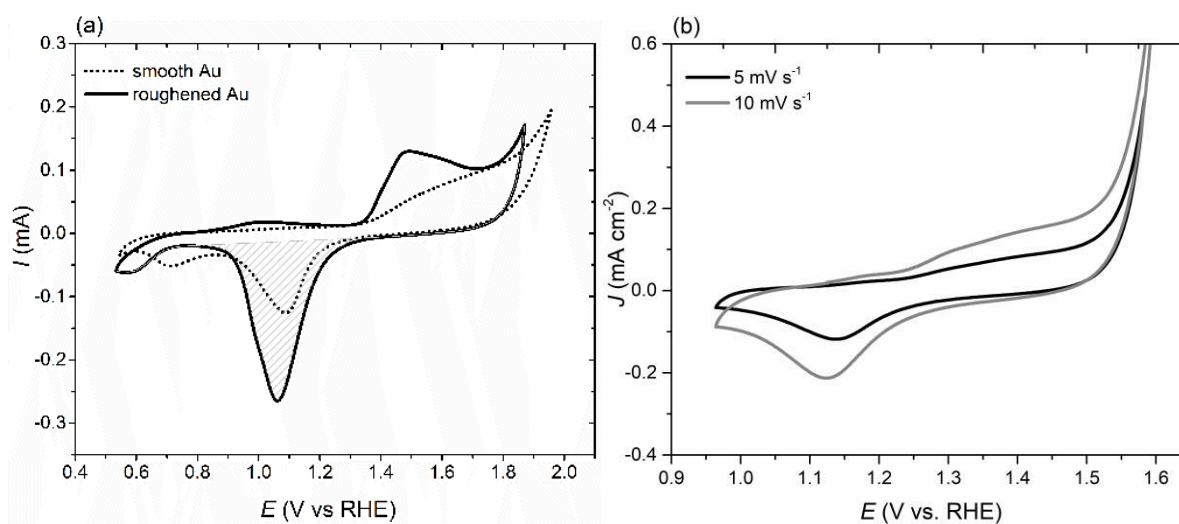

Figure S2. (a) Cyclic voltammetry of smooth and roughened gold surfaces in 0.1 M phosphate buffer solutions (pH 7.4, scan rate: 50 mV s^{-1}), (b) Cyclic voltammetry of nanostructured Au in 0.1 M Fe-free KOH (pH 13, $v = 5$, 10 mV s^{-1}).

Table S1. Real surface area of Au electrodes

	Q_{AuO} (μC)	ECSA $= \dfrac{Q_{AuO}{}^{a}}{Q_{Au}{}^{b}}$	Roughness^{c}	% Increase of ECSA
smooth Au	422	0.880	4.50	
				53%
roughened Au	896	1.860	9.50	

^{a} corresponds to the integrated charge of the reduction peak of the gold oxide.
^{b} theoretical value of the mean surface concentration of gold atoms on a smooth surface.
^{c} the roughness is calculated by dividing the ECSA with the geometric surface area of the electrodes, which is equal to 0.196 cm^{2}.

2.2. Thin films of cobalt oxyhydroxide

The real surface area of cobalt oxyhydroxide electrodeposited on roughened gold substrates was determined by both cyclic voltammetry and electrochemical impedance measurements (EIS described in section S5). Figure S3a shows the polarisation curves at the potential window 1.255 V–1.345 V vs. RHE, where the observed charging current corresponds to the double-layer capacitance with respect to the scan rate (10, 20, 50, 100, 150, 200 mV s^{-1}). Plots of the difference of the anodic and cathodic current densities, $\Delta J = |j_a - j_c|$, at 1.30 V vs. RHE versus the scan rate are shown in Figure S3b. The C_{dl} is equal to one half of the slope of the fitted data in Fig. 3b. The ECSA is determined by dividing the C_{dl} with the specific capacitance, C_s, assuming a specific capacitance of 40 µF cm^{-2}.[2] The roughness factor was determined by dividing this ECSA with the geometric area of the electrode.
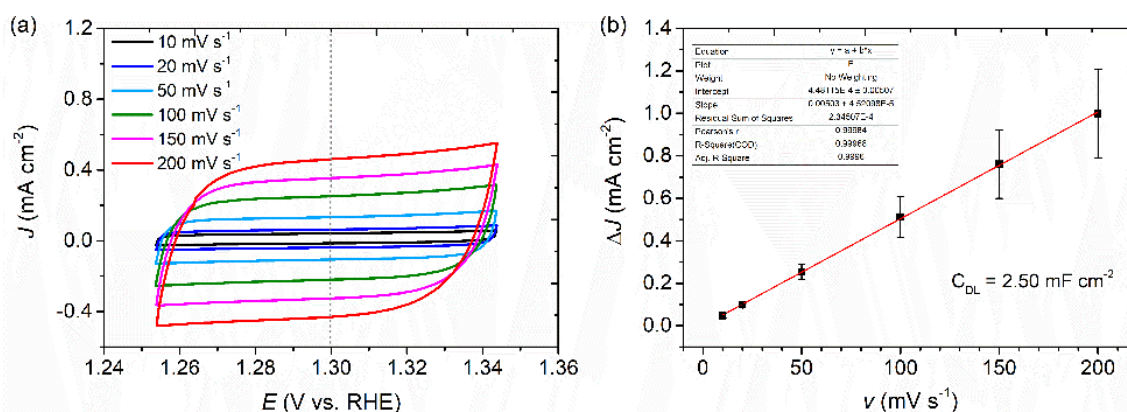

Figure S3. (a) Cyclic voltammograms of cobalt oxyhydroxide in 0.1 M Fe-free KOH at different scan rates (10. 20, 50, 100, 150, 200 mV s^{-1}) for the determination of the C_{dl}, (b) plots of the difference of the anodic and cathodic current densities, $\Delta J = |j_a - j_c|$, versus the scan rate v (10, 20, 50, 100, 150, 200 mV s^{-1}). The double-layer capacitance is equal to 2.50±0.60 mF cm^{-2}. The values are the means of three different samples; error bar designates standard deviation.

The determination of ECSA through measuring non-faradaic double-layer capacitance, C_{dl}, have some inherent uncertainties.[2,3] The conversion of C_{dl} to ECSA can be ambiguous and complicated by different surface morphologies. Moreover, dynamic complexity in electrochemical reactions, where not only double layer charging but various ion transfer reactions such as specific adsorption and intercalation of electrolyte ions, leads to the inaccuracy of C_{dl}-derived ECSA. Poor conductivity of insulating oxides also contributes to inaccurate ECSA estimation due to dielectric behavior.[4–6] We determined the C_{dl} at 1.55 V vs RHE by the EIS response of the system and by cyclic voltammetry at the potential range 1.255 V–1.345 V where our Co film is conductive.[7] The results from two different methods are close, suggesting a relative robustness of our methods.
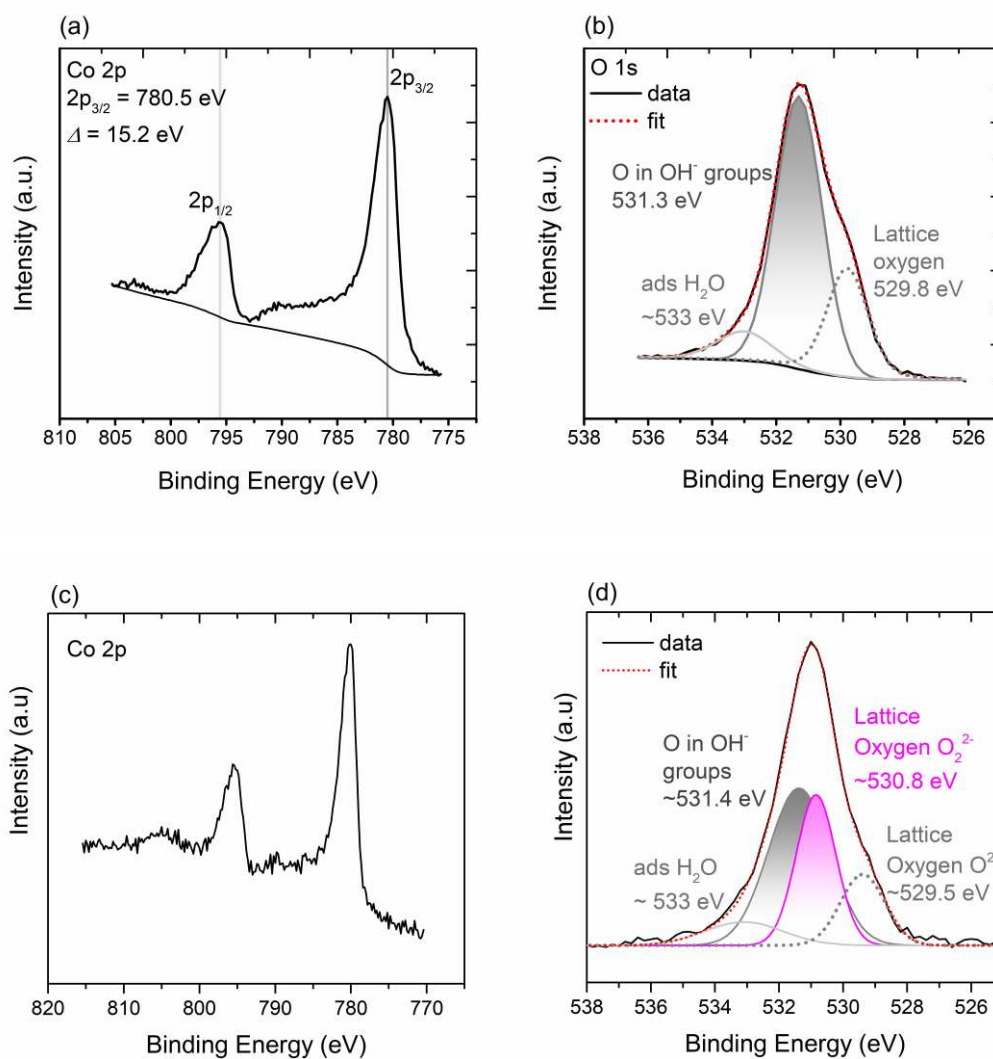
3. X-ray photoelectron spectroscopy

Figure S4. (a, c) Co 2p and (b, d) O 1s X-ray photoelectron spectra of (a,b) as-prepared CoOOH, and (c, d) after-electrolysis sample. For c and d, the as-prepared sample was subjected to a three-hour galvanostatic electrolysis at 5 mA cm^{-2}.

4. Electrochemical impedance spectroscopy

EIS measurements were conducted to determine the ECSA of the as-prepared cobalt oxyhydroxide films and to study the electrochemical properties of the catalyst as a function of the applied potential. The equivalent circuit used to model the EIS data was the Randles circuit shown in Figure S5b.[5,8,9] The circuit comprises three circuit elements: a resistor (R_e) for the electrolyte resistance, a resistor (R_{ct}) related to the charge-transfer resistance of an electrochemical process, and a constant phase element, CPE, which simulates the double-layer capacitance.[10] The CPE has two degrees of freedom; (i) the coefficient, Q, related to the electrode capacitance, and (ii) the constant phase exponent, α. For $\alpha = 1$, the EIS response is that of an ideal parallel capacitor. For $0 < \alpha < 1$, the behavior of the double-layer capacitance deviates from ideality dependent on the surface roughness and dispersion of the frequency.[4,8] Based on an equation of Brug et. al.[10], the double-layer capacitance can be estimated:

$$C_{dl} = \left[Q * \left(\frac{1}{R_e} + \frac{1}{R_{ct}} \right)^{(a-1)} \right]^{\frac{1}{a}} \quad (1)$$

where C_{dl} is the interfacial capacitance

Q the CPE coefficient,

α the constant phase component $(0 < \alpha < 1)$,

R_e the electrolyte resistance,

R_{ct} the charge transfer resistance.

The characteristic time constant (τ, s) of the charge transfer process is the product of the charge transfer resistance (R, Ω) and the double-layer capacitance (C, F), i.e., $\tau = RC$. The time constant decreases with increasing applied potential indicating a faster charge transfer process at the CoO_x–electrolyte interface (Figure S6).
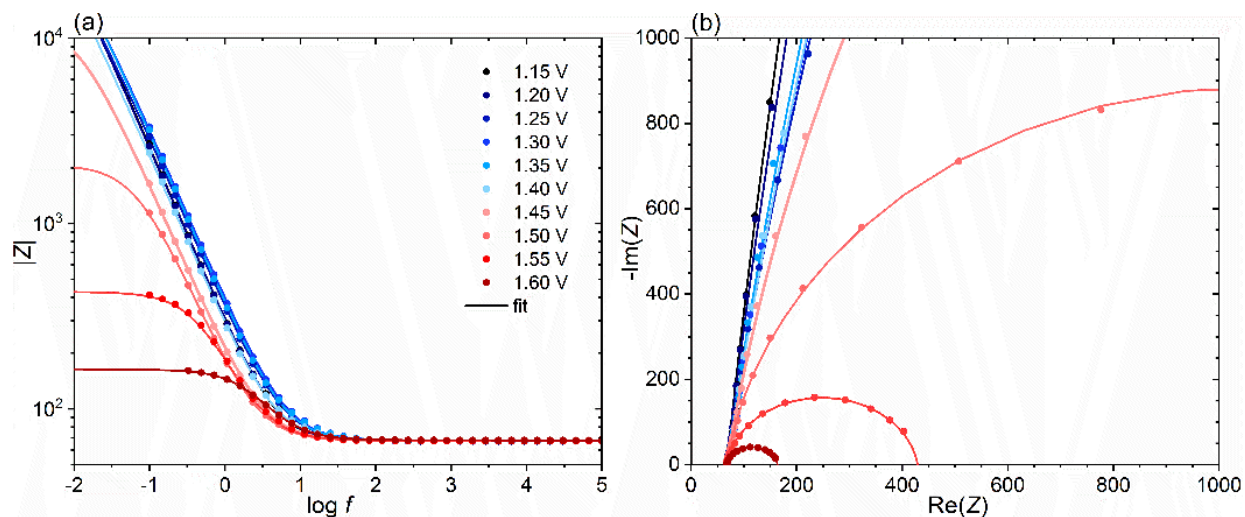
Figure S5. (a) Bode, and (b) Nyquist plots of cobalt oxyhydroxide in 0.1 M Fe-free KOH. The EIS response was recorded at different applied potentials to probe the electrochemical properties of the catalyst. The fitting of EIS data was performed using the Randles circuit depicted inside the Nyquist plot.
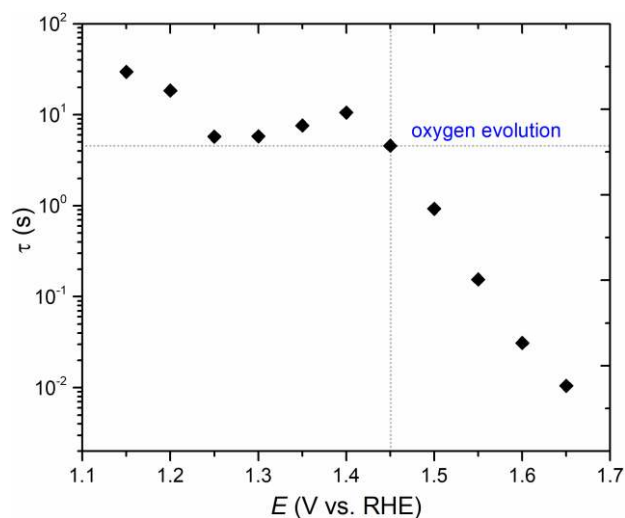

Figure S6. Characteristic time constant (τ, s) of the charge transfer process with respect to the applied potential (E, V). Under strong OER potentials (1.65 V), the characteristic time constant of the faradaic process is ca. 0.01 s in 0.1 M Fe-free KOH.

Water oxidation starts at potentials over 1.45 V vs. RHE, according to results shown in Figure S5a, b, and S6.

Table S2. ECSA determination of thin films of CoOOH

Method	C_{dl} (mF cm^{-2})	ECSA (cm^2)[c]	RF[d]
Cyclic Voltammetry	2.50±0.60[a]	12.30±2.90	63±15
EIS	2.80±0.60[b]	13.70±2.90	70±15

[a] The double-layer capacitance (per geometric surface area) was calculated at the potential range 1.20–1.65 V vs. RHE and the values reported here are at 1.55 V vs. RHE.
[b] Based on the fitting of the EIS data at 1.55V vs. RHE
[c] The ECSA was calculated by dividing the C_{dl} with a specific capacitance of 40 µF cm^{-2}
[d] The Roughness Factor is calculated by dividing the ECSA with the geometric surface area of the electrode (equal to 0.196 cm^2)

The very small thickness of our catalysts (ca. 2.0–2.5 nm) deposited on a high surface area Au substrate resulted in a low-resistance Au-film contact, where the resistance of the film to electron transfer seems negligible. For this reason, we chose the Randles circuit for fitting the EIS response. As expected, the Nyquist plot exhibits one semicircle related to the charge-transfer process at the electrolyte/catalyst interface.

5. EXAFS fitting

EXAFS curve fitting was performed with REX2000 software using *ab initio*-calculated phases and amplitudes from the program FEFF 8.2. These *ab initio* phases and amplitudes were used in the EXAFS equation

$$\chi(k) = S_0^2 \sum_j \frac{N_j}{kR_j^2} f_{eff_j}(\pi,k,R_j) e^{-2\sigma_j^2 k^2} e^{-2R_j/\lambda_j(k)} \sin(2kR_j + \phi_{ij}(k))$$

   The neighboring atoms to the central atom(s) are divided into j shells, with all atoms with the same atomic number and distance from the central atom grouped into a single shell. Within each shell, the coordination number N_j denotes the number of neighboring atoms in shell j at a distance of R_j from the central atom. $f_{eff_j}(\pi,k,R_j)$ is the *ab initio* amplitude function for shell j, and the Debye-Waller term $e^{-2\sigma_j^2 k^2}$ accounts for damping due to static and thermal disorder in absorber-backscatter distances. The mean free path term $e^{-2R_j/\lambda_j(k)}$ reflects losses due to inelastic scattering, where $\lambda_j(k)$ is the electron mean free path. The oscillations in the EXAFS spectrum are reflected in the sinusoidal term $\sin(2kR_j + \varphi_{ij}(k))$, where $\varphi_{ij}(k)$ is the *ab initio* phase function for shell j. S_0^2 is an amplitude reduction factor due to shake-up/shake-off processes at the central atom(s). The EXAFS equation was used to fit the experimental data using CN, R, and the EXAFS Debye-Waller factor (DW; σ^2) as variable parameters. For the energy (eV) to wave vector (k, Å^{-1}) axis conversion, the S_0^2 value was determined as 0.90. All fits were performed in the R space.
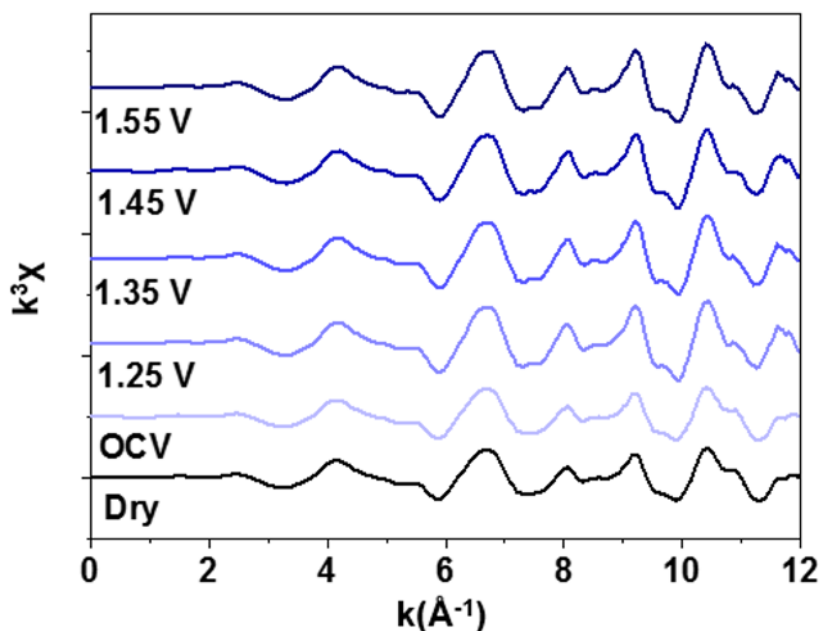

Figure S7. In situ k^3-weighted EXAFS K-space spectra under various conditions.
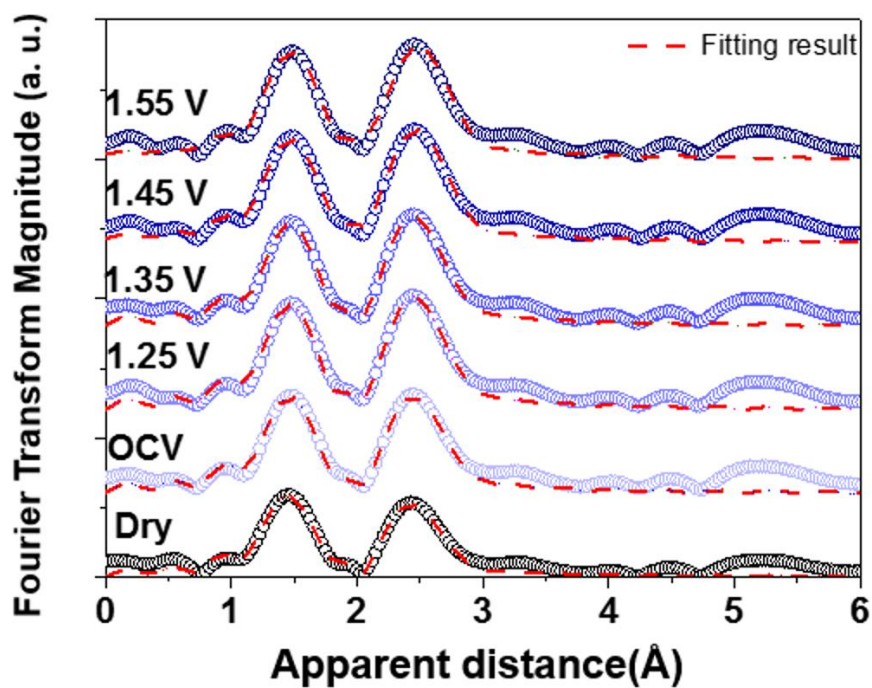
Figure S8. In situ EXAFS R-space spectra with fitting curves under various conditions.

Table S3. Fitting result of EXAFS.

condition	path	R (Å)	N	ΔE (eV)	σ² (Å²)	R factor
dry	Co-O	1.90(3)	4.6(6)	-3.5(6)	0.0040(6)	1.316
	Co-Co	2.83(4)	4.5(5)	-4.2(7)	0.0058(4)	
OCV	Co-O	1.90(3)	5.5(7)	-2.3(5)	0.0045(4)	1.832
	Co-Co	2.84(3)	5.1(5)	-3.7(6)	0.0047(9)	
1.25V	Co-O	1.89(4)	5.6(6)	-2.2(5)	0.0044(4)	2.011
	Co-Co	2.84(3)	5.5(3)	-3.2(5)	0.0042(8)	
1.35V	Co-O	1.89(4)	5.7(7)	-1.9(5)	0.0042(6)	1.665
	Co-Co	2.84(4)	5.6(4)	-3.5(6)	0.0047(7)	
1.45V	Co-O	1.87(4)	6.0(6)	1.2(5)	0.0047(4)	1.636
	Co-Co	2.84(3)	5.7(5)	-2.2(5)	0.0047(7)	
1.55V	Co-O	1.86(3)	6.0(7)	4.4(5)	0.0045(4)	1.592
	Co-Co	2.84(3)	5.7(4)	-2.1(5)	0.0045(8)	

6. In situ surface-enhanced Raman spectroscopy

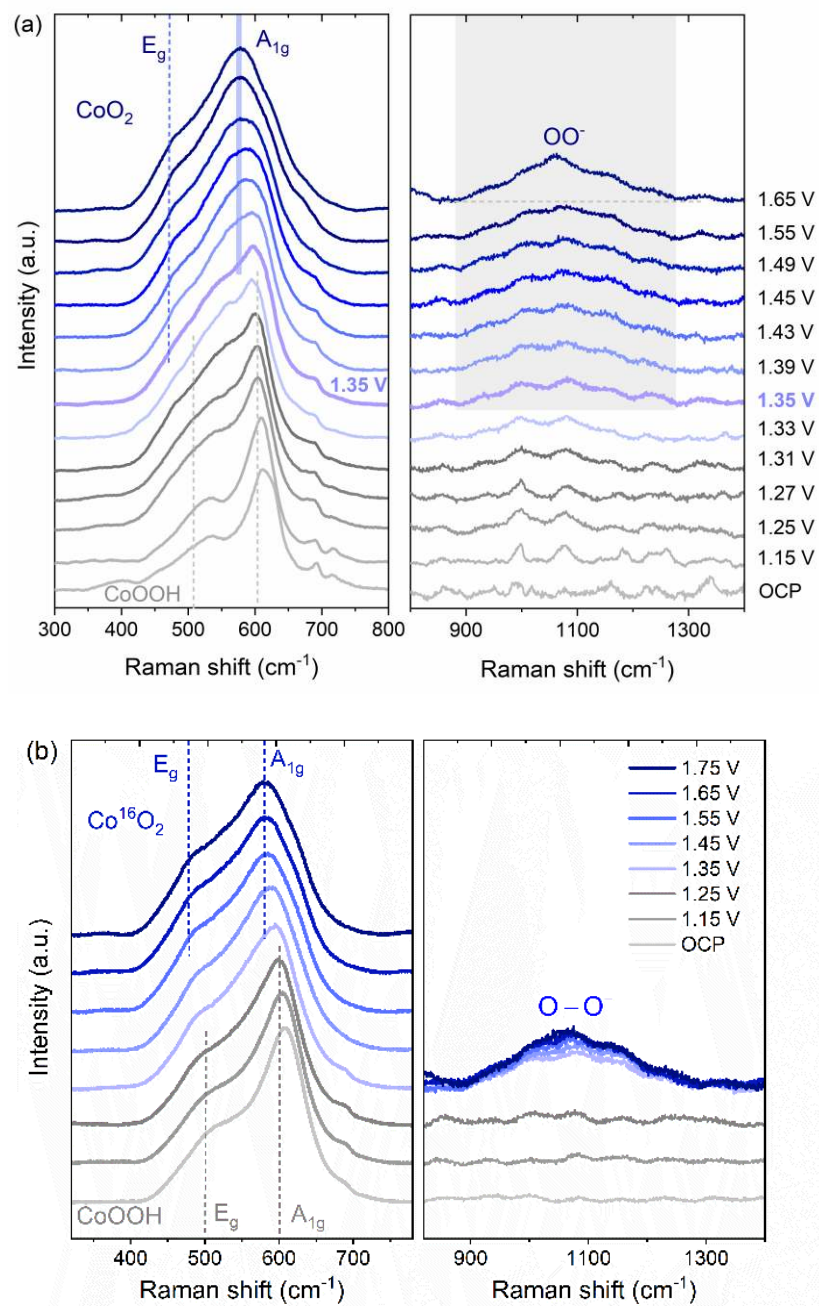### 6.1. In situ SERS in ^{16}O-KOH

Figure S9. (a) In situ Raman peaks of Co^{16}OOH in 0.1 M Fe-free ^{16}O-KOH at increasing applied potential, (b) Increasing Raman intensity of the broad band at about 1075 cm^{-1} with increasing applied potential.

The Raman spectra of as-prepared Co_3O_4, $LiCoO_2$, and $Co(OH)_2$ were collected as reference compounds. The Raman peaks are different from the as-prepared CoOOH as expected.

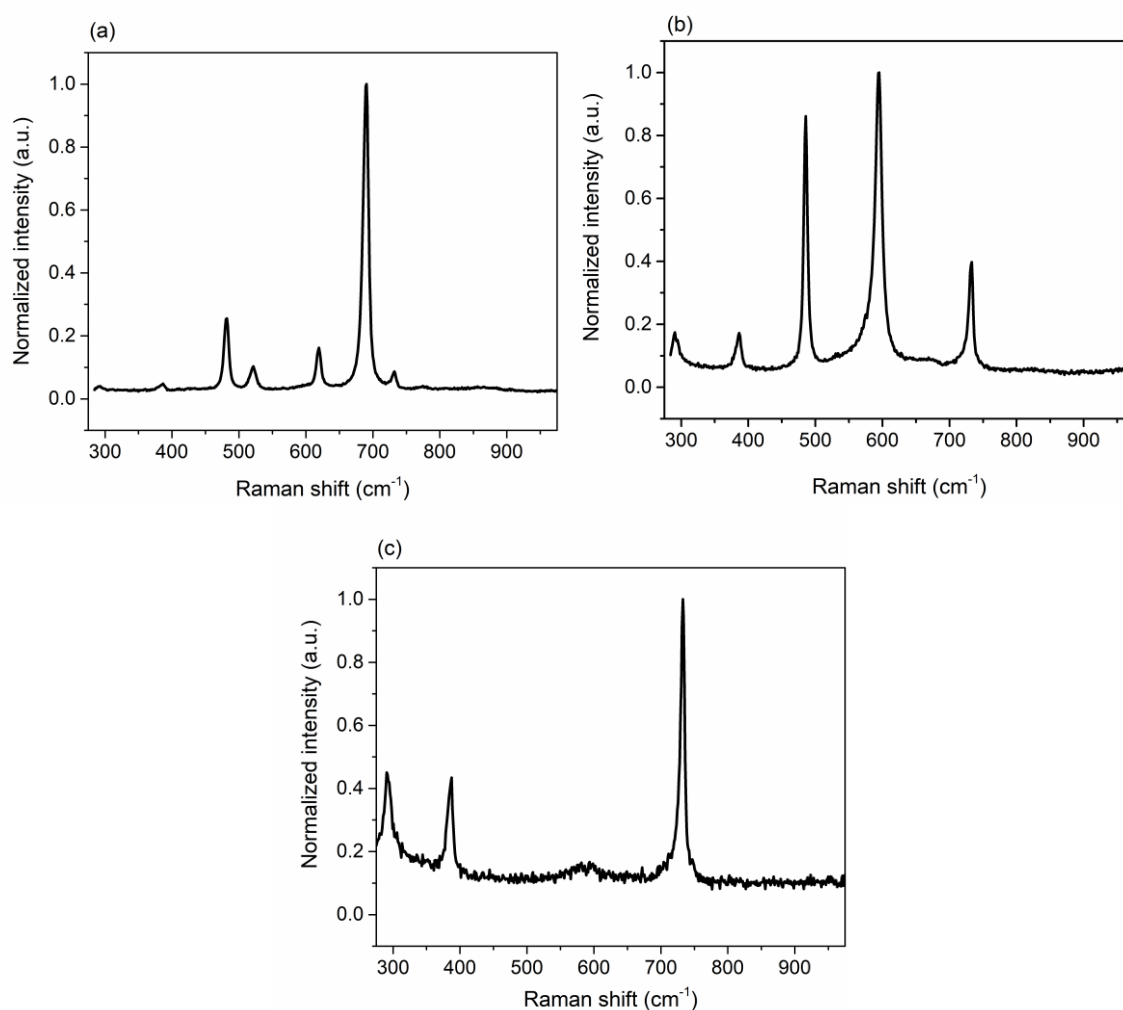**Figure S10.** Raman spectra of the reference compounds (a) Co_3O_4, (b) $LiCoO_2$, (c) $Co(OH)_2$ under dry conditions.
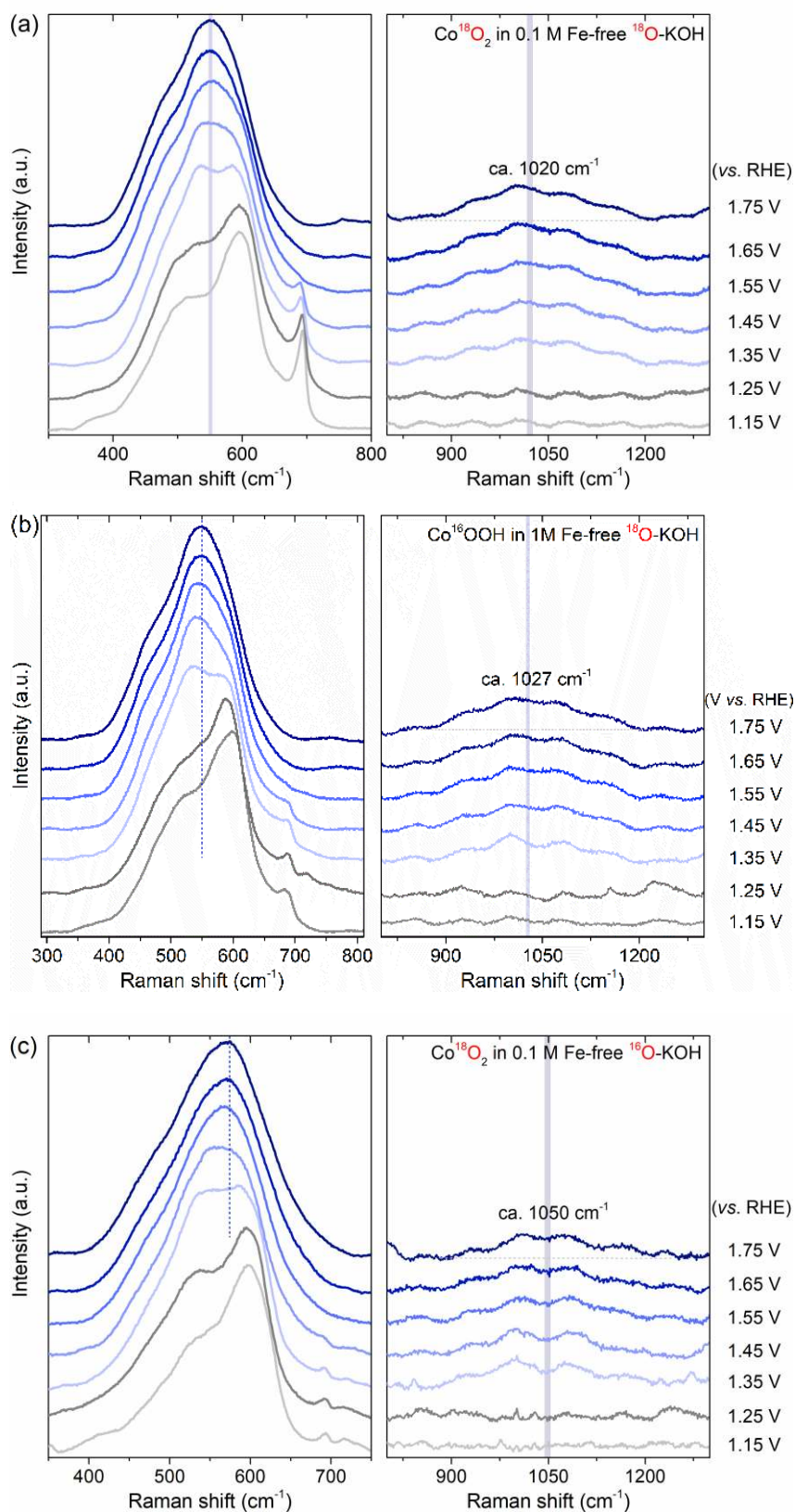
Figure S11. In situ Raman spectra on roughened Au substrates of; (a) $Co^{18}O_2$ in 0.1 M Fe-free ^{18}O-KOH, (b) $Co^{16}OOH$ in 0.1 M Fe-free ^{18}O-KOH, and (C) $Co^{18}O_2$ in 0.1 M Fe-free ^{16}O-KOH. The freshly prepared $Co^{16}OOH$ were labelled with ^{18}O by steady state electrolysis at 1.75 V for 10 min.

7. Calculation of Co atoms in the film

CoOOH films were electrodeposited anodically by applying a constant current equal to 10 µA for 3 min.

i. **The maximum charge** involved for deposition is calculated as:

10 A (10^{-6}) x 180 s x 6.02 x 10^{23} mol^{-1}/ 96485.3 C mol^{-1} = 1.123 10^{16} electrons.

During the oxidative deposition, Co(II) was oxidized to Co(III) (assuming CoOOH as the formed film). That means 1 e^{-} consumed per Co atom, so theoretically this corresponds to **1.123 10^{16} Co atoms deposited.**

ii. **From ICP-OES**, we have 77.00±6.30 µg/L or 1.310±0.110 nmol/mL. The total volume analysed was 0.01L, which leads us to **13.10±1.10 nmol of Co atoms** deposited during the deposition.

The number of Co atoms electrodeposited on the Au surface is then equal to 13.10 nmol x N_A atoms/mol = **0.8097 x 10^{16} Co atoms**. As expected, the total number of Co atoms electrodeposited is smaller than the one calculated by the maximum anodic charge.

In the total loading of CoOOH, there are 2 x n_t(Co) = **26.20±2.20 nmol of O atoms** or **1.6194 x 10^{16} O atoms.**

iii. **Calculation of Co surface atoms based on ECSA experiments:**

Given that the ECSA is ca. 12.30±2.90 cm^2 and the Esswein estimation of 6.1 x 10^{14} surface Co atoms/cm^2,[11,12] we can calculate **12.50±2.90 nmol of surface Co atoms** or **0.750±0.176 x10^{16} surface Co atoms**. This means that 95% of the total Co atoms deposited are surface atoms.

Assuming CoOOH as phase, there are 2 x n_t(Co) = **25.00±5.80 nmol of O atoms** or 1.512 x 10^{16} O atoms.

iv. **By intergrading the oxidation peak** of Co(III) to Co(IV) between 1.30 and 1.57 V vs RHE (Figure 1), we found a total anodic charge equal to **0.584 mC cm^{-2}**, which corresponds to **1.50 nmol of Co or 0.0912 x 10^{16} surface Co atoms**. This corresponds **to ca. 12% of the total surface Co atoms** (with respect to the total number of surface atoms based on the ECSA). Baltruschat et. al[13] calculated previously that 12% of the surface cobalt atoms are catalytically active in the case of 50 nm thick Co_3O_4.

Assuming CoO_2, we can calculate **3.02 nmol of O atoms.**

v. **Labelling process:** Fresh Co^{16}OOH is subjected to electrolysis at 1.75 V vs. RHE in ^{18}O-KOH:

Total charge consumed is equal to 3,165 mC cm^{-2} or 621 mC. This corresponds to 621 mC/4F = **1,609 nmol of O_2 released** → 3,218 nmol of O atoms. Enough to label all the lattice oxygen.

vi.   The labelled $Co^{18}O_2$ is subjected to potentiostatic electrolysis in ^{16}O-KOH:

  a.   At 1.45 V vs. RHE: total charge consumed 13.98 mC cm^{-2} or 2.74 mC. This corresponds to 2.74 mC/4F = **7.11 nmol of O₂ released** → 14.<u>22 nmol of O atoms</u>.

  b.   At 1.55 V vs. RHE: total charge consumed 62.79 mC cm^{-2} or 12.32 mC. This corresponds to about **31.92 nmol of O₂ released** → 63.84 <u>nmol of O atoms</u>.

  c.   At 1.65 V vs. RHE: total charge consumed 1,057mC cm^{-2} or 207.44 mC. This corresponds to about 537.50 **nmol of O₂ released** → 1,075 <u>nmol of O atoms</u>.

  d.   At 1.75 V vs. RHE: total charge consumed 3,169 mC cm^{-2} or 622. This corresponds to about 1,611 **nmol of O₂ released** → 3,223 <u>nmol of O atoms</u>.

According to these calculations, the charge passed should be sufficient to enable all the lattice oxygen atoms to exchange fully in OER. Yet, not all the ^{18}O of the labelled $Co^{18}O_2$ was exchanged even after prolonged electrolysis.
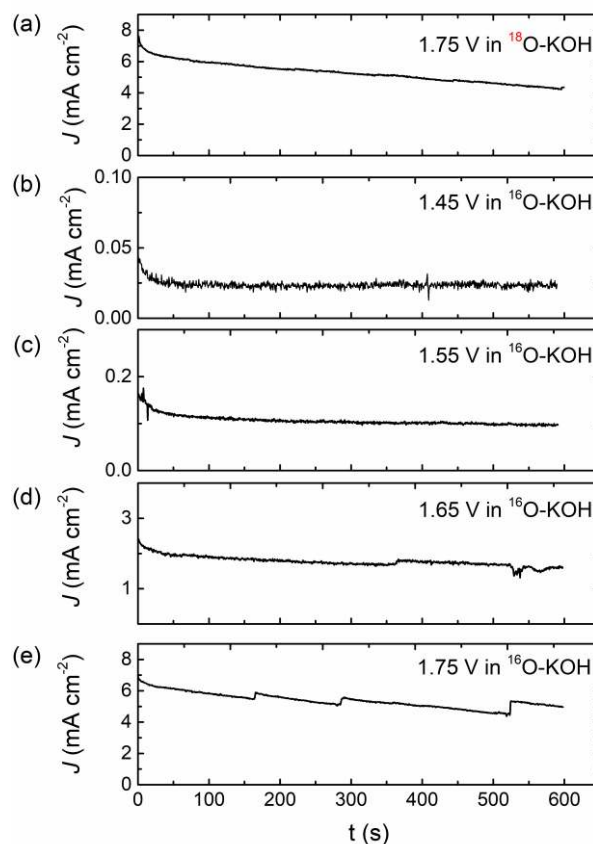

Figure S12. Typical profiles during potentiostatic electrolysis (a) at 1.75 V vs RHE in 0.1 M Fe-free ^{18}O-KOH, and (b-e) from 1.45 to 1.75 V vs. RHE in 0.1 M Fe-free ^{16}O-KOH.
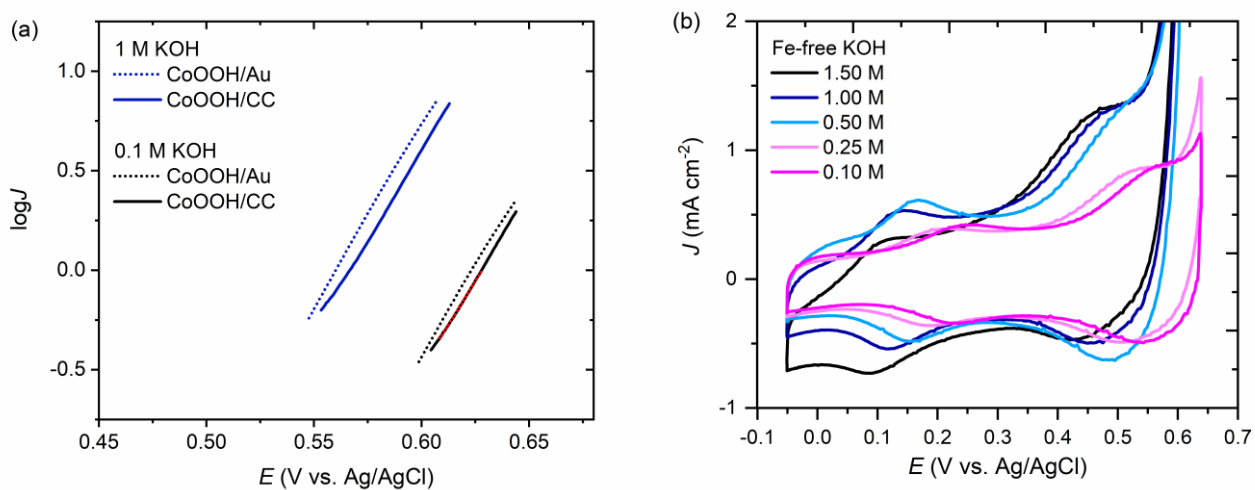
8. Electrokinetic study

Figure S13. (a) Tafel plots of CoOOH on Au and Carbon Cloth substrates in 1 M and 0.1 M Fe-free KOH solutions, (b) cyclic voltammograms of CoOOH on Carbon Cloth in Fe-free KOH solutions (1.50 M, 1.00 M, 0.50 M, 0.25 M, 0.10 M).

Table S4. Tafel slope with respect to the pH

[OH⁻] (M)	b^i (mV dec^{-1})	s^{ii}
1.50	59.4	0.3
1.00	58.9	1.7
0.50	59.1	2.3
0.25	59.5	0.3
0.10	60.9	2.6
0.05	58.0	1.6
0.01	59.1	0.7

^{i} The mean values are the average of three different samples.
^{ii} standard deviation

9. H/D isotope experiment

Isotopic experiments were carried out in deuterated water in order to elucidate the role of deprotonation steps in the catalytic cycle. Comparing the catalytic activity in H_2O and D_2O, we observe an anodic shift of the potential (ca. 30 mV) required to produce 1 mA cm^{-2}. Cyclic voltammetry in H_2O and D_2O shows a same order anodic shift of the redox potentials in D_2O. This indicates that the decrease of the catalytic current in deuterated water is linked to the anodic shift of the Co(III/IV) redox event.

Table S5. Tafel slope with respect to the pD

[OD⁻] (M)	b[i] (mV dec⁻¹)	s[ii]
1.00	60.1	1.5
0.50	60.9	1.4
0.25	58.7	0.6
0.10	58.5	0.4

[i] The mean values are the average of three different samples. [ii] standard deviation
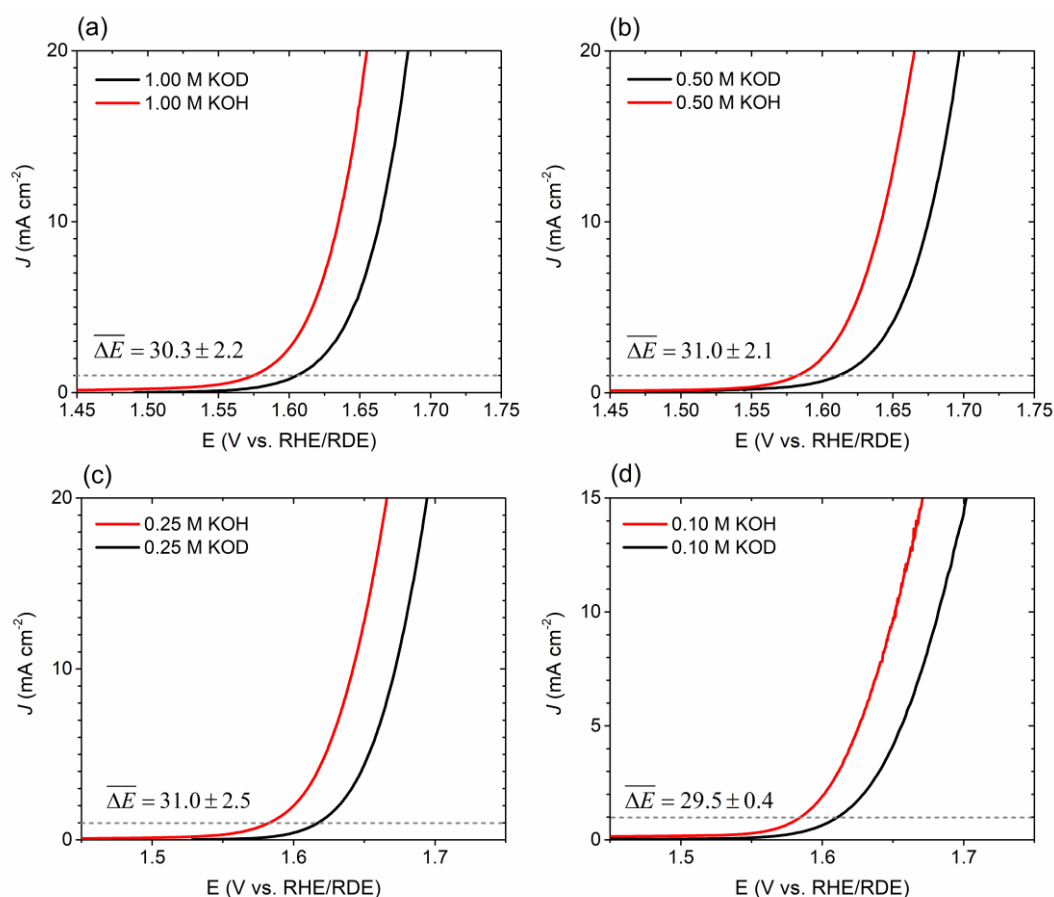

Figure S14. LSV curves of CoOOH recorded in Fe-free KOH and KOD solutions of various concentrations (1.0, 0.5, 0.25, 0.10 M). Conditions: Carbon cloth, 1 mV s⁻¹. For the calculation of RDE scale, 0.87 units were added in the pH values of the KOH solutions.
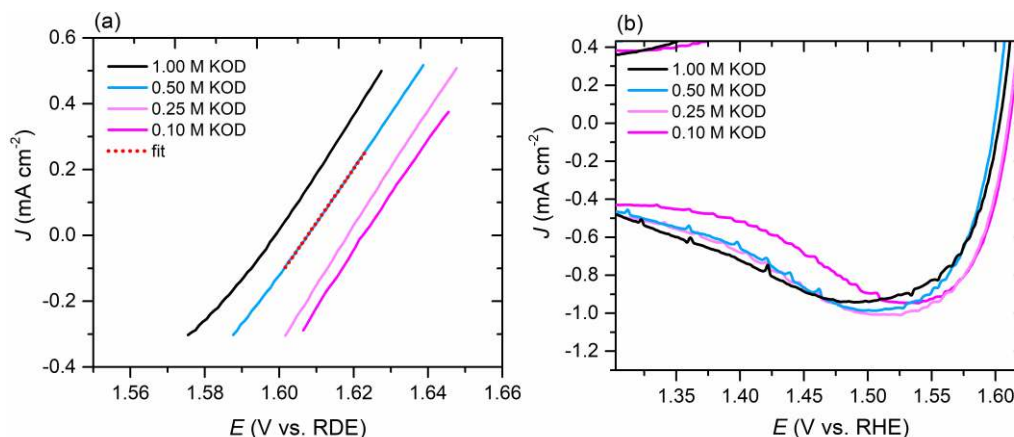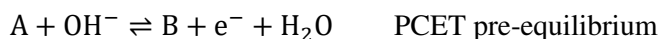
Figure S15. (a) Tafel plots of cobalt oxyhydroxide in 1.00, 0.50, 0.25, 0.10 M Fe-free KOD (scan rate: 1 mV s⁻¹), and (b) the reduction peak of Co(III)/Co(IV) redox couple recorded in KOD by cyclic voltammetry at 100 mV s⁻¹ scan rate.

10. Electrokinetic model

The concept of quasi-equilibrium can be used as an approach to study the mechanism of multi-step electrochemical reaction.[14–17] Given the dependency of an electrochemical rate constant on potential, we can assume that there must be one distinguishable rate-determining step (RDS) controlling the overall rate of the sequence at a specific potential window.[14,15] That means that all the steps prior and after the RDS proceed at a much slower rate than what they could and can be regarded at equilibrium.

$$A + OH^- \rightleftharpoons B + e^- + H_2O \qquad \text{PCET pre-equilibrium}$$

$$B \xrightarrow{k_2} C \qquad\qquad\qquad \text{pure chemical RDS}$$

The rate of the RDS and pre-equilibrium step can be expressed as:

RDS: $\qquad\qquad v = k_2\theta$

Pre-equilibrium: $\qquad v_1 = k_1 a_{OH^-}(1-\theta)\exp\left(\frac{\beta\eta F}{RT}\right)$ (forward reaction)

$$v_{-1} = k_{-1}\theta\exp\left(-\frac{(1-\beta)\eta F}{RT}\right) \quad \text{(backward reaction)}$$

Where k_2 the rate constant of the RDS, k_1 and k_{-1} the electrochemical rate constants of the forward and backward reactions, respectively, θ is the partial surface coverage of the intermediate B, and β is the symmetry factor of forward reaction.

Since we are at equilibrium, the rates of the forward and backward reactions are equal:

$$v_1 = v_{-1}$$

$$\frac{\theta}{1-\theta} = \frac{k_1}{k_{-1}}a_{OH^-}\exp\left(\frac{\eta F}{RT}\right)$$

For low coverage $\theta \ll 1$, the rate of the overall reaction is governed by the following equation:

$$v = k_2\frac{k_1}{k_{-1}}a_{OH^-}\exp\left(\frac{\eta F}{RT}\right) = k_2k_1a_{OH^-}\exp\left(\frac{\eta F}{RT}\right)$$

The current density of the OER process is then described by:

$$i = 4Fv = 4Fk_2K_1a_{OH^-}\exp\left(\frac{\eta F}{RT}\right) = i_o\exp\left(\frac{\eta F}{RT}\right)$$

$$\log i = \log i_o + \frac{\eta}{b}$$

Tafel slope: $b = \frac{\partial \eta}{\partial \log i} = 2.303\frac{RT}{F} = 60\,mV/dec$

11. References

(1)   Oesch, U.; Janata, J. Electrochemical Study of Gold Electrodes with Anodic Oxide Films—I. Formation and Reduction Behaviour of Anodic Oxides on Gold. Electrochimica Acta **1983**, 28 (9), 1237–1246.

(2)   Jung, S.; McCrory, C. C. L.; Ferrer, I. M.; Peters, J. C.; Jaramillo, T. F. Benchmarking Nanoparticulate Metal Oxide Electrocatalysts for the Alkaline Water Oxidation Reaction. J. Mater. Chem. A **2016**, 4 (8), 3068–3076.

(3)   Wei, C.; Rao, R. R.; Peng, J.; Huang, B.; Stephens, I. E. L.; Risch, M.; Xu, Z. J.; Shao-Horn, Y. Recommended Practices and Benchmark Activity for Hydrogen and Oxygen Electrocatalysis in Water Splitting and Fuel Cells. Adv. Mater. **2019**, 31 (31), 1806296.

(4)   Doyle, R. L.; Godwin, I. J.; Brandon, M. P.; Lyons, M. E. G. Redox and Electrochemical Water Splitting Catalytic Properties of Hydrated Metal Oxide Modified Electrodes. Phys. Chem. Chem. Phys. **2013**, 15 (33), 13737–13783.

(5)   Chakthranont, P.; Kibsgaard, J.; Gallo, A.; Park, J.; Mitani, M.; Sokaras, D.; Kroll, T.; Sinclair, R.; Mogensen, M. B.; Jaramillo, T. F. Effects of Gold Substrates on the Intrinsic and Extrinsic Activity of High-Loading Nickel-Based Oxyhydroxide Oxygen Evolution Catalysts. ACS Catal. **2017**, 7 (8), 5399–5409.

(6)   Batchellor, A. S.; Boettcher, S. W. Pulse-Electrodeposited Ni–Fe (Oxy)Hydroxide Oxygen Evolution Electrocatalysts with High Geometric and Intrinsic Activities at Large Mass Loadings. ACS Catal. **2015**, 5 (11), 6680–6689.

(7)   Burke, M. S.; Zou, S.; Enman, L. J.; Kellon, J. E.; Gabor, C. A.; Pledger, E.; Boettcher, S. W. Revised Oxygen Evolution Reaction Activity Trends for First-Row Transition-Metal (Oxy)Hydroxides in Alkaline Media. J. Phys. Chem. Lett. **2015**, 6 (18), 3737–3742.

(8)   L. Doyle, R.; G. Lyons, M. E. An Electrochemical Impedance Study of the Oxygen Evolution Reaction at Hydrous Iron Oxide in Base. Phys. Chem. Chem. Phys. **2013**, 15 (14), 5224–5237.

(9)   Moysiadou, A.; Hu, X. Stability Profiles of Transition Metal Oxides in the Oxygen Evolution Reaction in Alkaline Medium. J. Mater. Chem. A **2019**, 7 (45), 25865–25877.

(10)   Brug, G. J.; van den Eeden, A. L. G.; Sluyters-Rehbach, M.; Sluyters, J. H. The Analysis of Electrode Impedances Complicated by the Presence of a Constant Phase Element. J. Electroanal. Chem. Interfacial Electrochem. **1984**, 176 (1), 275–295.

(11)   Esswein, A. J.; McMurdo, M. J.; Ross, P. N.; Bell, A. T.; Tilley, T. D. Size-Dependent Activity of Co3O4 Nanoparticle Anodes for Alkaline Water Electrolysis. J. Phys. Chem. C **2009**, 113 (33), 15068–15072.

(12)   Yeo, B. S.; Bell, A. T. Enhanced Activity of Gold-Supported Cobalt Oxide for the Electrochemical Evolution of Oxygen. J. Am. Chem. Soc. **2011**, 133 (14), 5587–5593.

(13)   Amin, H. M. A.; Baltruschat, H. How Many Surface Atoms in Co3O4 Take Part in Oxygen Evolution? Isotope Labeling Together with Differential Electrochemical Mass Spectrometry. Phys. Chem. Chem. Phys. **2017**, 19 (37), 25527–25536.

(14)   Elizier Gileadi. Multi-Step Electrode Reactions. In Electrode Kinetics for Chemists, Chemical Engineers, and Material Scientists.; VCH Publishers, Inc.: New York, **1993**; pp 127–184.

(15)   Bockris, J. O. Kinetics of Activation Controlled Consecutive Electrochemical Reactions: Anodic Evolution of Oxygen. J. Chem. Phys. **1956**, 24 (4), 817–827.

(16)   Bockris, J. O.; Otagawa, T. Mechanism of Oxygen Evolution on Perovskites. J. Phys. Chem. **1983**, 87 (15), 2960–2971.

(17)   Surendranath, Y.; Kanan, M. W.; Nocera, D. G. Mechanistic Studies of the Oxygen Evolution Reaction by a Cobalt-Phosphate Catalyst at Neutral PH. J. Am. Chem. Soc. **2010**, 132 (46), 16501–16509.